A Versatile Silica Functionalization Strategy for Organic Phase Nanomaterials

Keisuke Nagao[1-3], Katherine Lei[1], Peyton Worthington[4], Noah Kent[2-3], Michika Onoda[1†], Elian Malkin[2,3,5], Emmanuel Vargas Paniagua[2,3], Rebecca Leomi[2,3], Robert J. Macfarlane[1,], and Polina Anikeeva[1-3,5,*]*

[1] Department of Materials Science and Engineering, Massachusetts Institute of Technology; Cambridge, MA 02139, USA

[2] Research Laboratory of Electronics, Massachusetts Institute of Technology; Cambridge, MA 02139, USA

[3] McGovern Institute for Brain Research, Massachusetts Institute of Technology; Cambridge, MA 02139, USA

[4] Department of Mechanical Engineering, Massachusetts Institute of Technology; Cambridge, MA 02139, USA

[5] Department of Brain and Cognitive Sciences, Massachusetts Institute of Technology; Cambridge, MA 02139, USA

* Correspondence addressed to: R. J. M. (rmacfarl@mit.edu) and P. A. (anikeeva@mit.edu)

Keywords: silica shell coating, reverse microemulsion method, magnetic nanoparticles, nanodiscs, quantum dots

Abstract

Chemical interactions between nanoparticles and their surroundings are governed by their surface chemistry. Therefore, a versatile strategy for surface functionalization that is compatible with a variety of particle compositions would empower nanotechnology research. Silica coating offers a promising approach, but the ease with which silica shells can be synthesized is determined by the initial solution state of the nanoparticle, since the silica sol-gel chemistry typically occurs in an aqueous phase. While protocols for coating water-soluble particles are well-established, protocols for nanomaterials suspended in organic solvents require phase-transfer during the coating process, often leading to inconsistent reproducibility, non-uniform thicknesses, difficulty in producing thin coatings, and particle aggregation during functionalization. Here, we demonstrate that these challenges stem from insufficient stabilization of the organic-phase particles during the phase transfer, and can be overcome by adding excess surface ligands during the silica growth process. The inclusion of these excess ligands sufficiently alters the nanoparticles' surface chemistry to suppress particle aggregation, allowing deposition of shells as thin as 0.7 nm on a wide range of nanoparticle compositions, sizes, and shapes. The versatility and reproducibility of this approach is illustrated through its application to isotropic magnetite nanoparticles with diameters between 20-28 nm, anisotropic magnetite nanodiscs >200 nm in diameter, and CdSe/ZnS quantum dots. These silica-coated nanomaterials retain their functional properties, and the silica shell can be further modified with application-specific organic moieties. This approach therefore provides a versatile means of stabilizing nanomaterials for applications that demand precise control over their surface chemistry independent of their functional properties.

1. Introduction

Controlling the surface properties of solution-dispersed nanomaterials is vital for ensuring their stability, processability, and uniformity in properties and functions.[1,2] These factors are particularly important for their applications in biological environments.[3] It is not uncommon for a nanomaterial with promising physical properties to be toxic without the appropriate surface chemistry,[4–13] and biomedical applications of nanomaterials often require functionalization with moieties that target specific cells or molecules.[14,15] Solution coatings are also useful in protecting or stabilizing nanoparticles in environments that would cause flocculation or chemical alteration of the nanoparticle compositions, thereby altering or degrading their physical properties. Examples include the photoluminescence of semiconductor quantum dots or perovskite nanoparticles,[16,17] the plasmonic properties of noble metal nanoparticles,[18] or the magnetic response of metal oxides.[19,20]

The diversity of compositions, geometries, and dimensions that gives rise to innumerable functional properties in nanomaterials poses a formidable challenge to engineering their surface properties, which often manifests in reinventing the functionalization procedures for each nanomaterial or target application. The encapsulation of nanomaterials with thin silica shells presents a promising solution for surface modification, since silica is fairly chemically inert, biologically compatible, and readily modified via further functionalization steps.[21–25] Indeed, several silica coating methods have been developed to enable nanoparticle protection or biocompatibility. However, the most robust techniques are predominantly applicable to water-dispersed particles, as the sol-gel condensation used to produce the silica coating takes place in the aqueous phase. In contrast, particles dispersed in organic solvents require a phase transfer step,

typically performed via the reverse microemulsion method (RMM).[11,26–30] The RMM method involves the exchange of nanoparticles' hydrophobic ligands with hydrolyzed tetraethyl orthosilicate (TEOS) and subsequent phase transfer from non-polar solvents to reverse water micelles in which the silica shell can grow. Since many types of nanomaterials are produced in organometallic colloidal syntheses that yield hydrophobic surface ligands, commonly oleylamine or oleic acid (OAc), the RMM is applicable to a wide range of colloidal nanoparticles.[31,32]

Despite their utility, RMM protocols are often challenging to reproduce and need to be adapted for each particle composition. Common failure modes are the production of empty silica spheres alongside the silica coated particles, or the aggregation of particles during coating to produce large, multicore silica-coated clusters (Figure 1a).[26,30,33] Thus, multiple RMM procedures have been reported for coating of nanoparticles with different compositions, each containing variations in reagents and reaction conditions.[24,26–28,30,34–36] These studies have advanced the fields of nanomaterials and colloids, and disparate design rules have been proposed to avoid the formation of empty silica spheres, such as matching the number of nanoparticles with reverse micelles or adjusting the total surface area of the nanoparticles.[27,37] Furthermore, the addition of excess surfactants or pre-treatment of particles to alter their ligand shell conformations have shown benefits in reducing the number of empty silica spheres or the formation of multicore clusters.[30,37] However, even with these advancements, it can still be challenging to reliably reproduce prior protocols when they are performed in new research environments or applied to novel particle compositions. Even with laborious optimization of protocols for emerging nanomaterials chemistries, multi-core aggregates often emerge thereby changing the balance between the number of nanoparticles and reverse micelles, breaking the design rules. A robust and straightforward

strategy to simplify the process of adapting these beneficial RMM silica coating approaches would minimize current bottlenecks in colloidal surface functionalization.

We hypothesized that the poor reproducibility of many RMM methods stems from the variation in the initial surface state of the particles being coated. The ligands (e.g. OAc) used to stabilize these particles in colloidal suspension bind to the particle surface dynamically, and thus the chemical reactions occurring during the silica growth process likely perturb the surface composition of the particles. As a result, much of the difficulty in replicating RMM protocols or translating them to new particle compositions may arise from the manner in which these differences affect ligand coatings during the RMM process. In fact, in the sol-gel condensation, ligand coatings prior to silica formation have been found critical to preventing aggregation during silica coating and to achieve uniform shells.[38–41] In RMM, although secondary co-surfactants have been used to alter the properties of micelles, these surfactants typically do not contain functional groups that bind strongly to the particles' surfaces.[42] Thus, they are not anticipated to significantly alter the composition of the ligand on nanomaterials itself and prevent aggregation. We therefore hypothesized that the incorporation of additional OAc directly to the silica shell coating solution would ensure that the ligand coating of nanomaterials remains saturated during RMM regardless of particle type, size, synthesis protocol, and particle batch in the same manner that ligand coatings do in the sol-gel method.[28,30,43] Here we demonstrate that the inclusion of additional ligand (as opposed to additional surfactant) allows nanomaterials to enter the reverse micelles individually, resulting in almost exclusively single-core particles. As the formation of multi-core aggregates is prevented, established design rules, such as number-based matching of the number of nanomaterials and reverse micelles, give one-to-one core-shells without the emergence of core-free silica spheres. This robust method, termed SCHLR (Silica Coating with Hydrophobic Ligands

in Reverse microemulsion), consistently produces uniform silica coatings on nanomaterials independent of their core chemistry or the integrity of their organic surface passivation.

Notably, the SCHLR method offers the formation of shells with thickness under 1 nm, which was previously unattainable with RMM methods due to aggregation of nanomaterials.[33,44] SCHLR can be applied to a variety of sizes and compositions of nanomaterials, and can be subsequently followed with a wealth of robust silica-functionalization chemistries to link targeting moieties. The SCHLR method therefore holds promise as a facile, reproducible, and universal method for silica shell coating of nanomaterials.

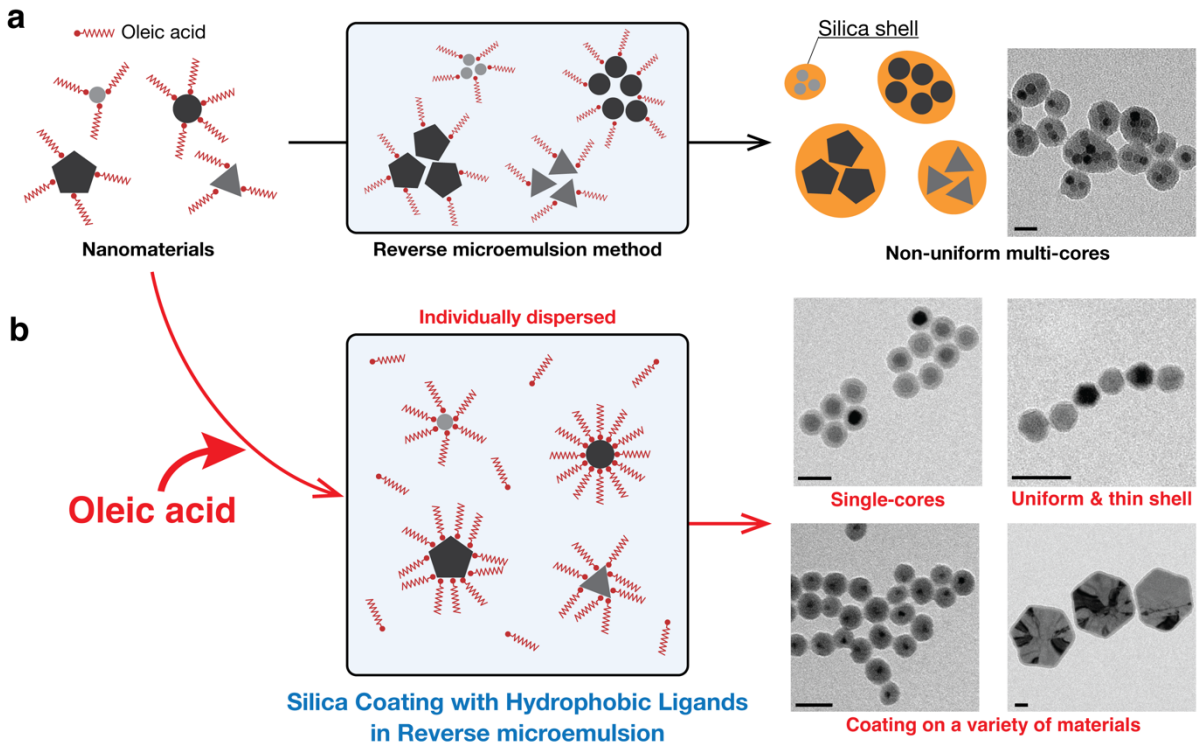

Figure 1. (a) Illustration of challenges in silica coating of nanomaterials via RMM. **(b)** Illustration of silica shell coating via Silica Coating with Hydrophobic Ligands in Reverse microemulsion (SCHLR) that is reproducible and agnostic toward nanomaterial core chemistry, size, or geometry. Scale bars, 50 nm.

2. Materials and Methods

All reagents and materials were purchased from Sigma-Aldrich unless otherwise mentioned and used as received. A brief description of the experimental protocols is included below, and detailed procedures and protocols (including information to aid in replication of results) are included in the Supplementary Methods.

2.1. Magnetic nanoparticle synthesis

Magnetic nanoparticles (MNPs) of Fe_3O_4 (magnetite) were synthesized using the thermal decomposition method.[45] As a precursor, iron oleate was synthesized from sodium oleate and $FeCl_3 \cdot 6H_2O$.[46] 123 mmol of sodium oleate (TCI Chemicals) and 40 mmol $FeCl_3 \cdot 6H_2O$ were heated in a 250-mL three-neck flask in a 70 ºC oil bath in a mixture of 100 mL hexane, 50 mL ethanol, and 50 mL DI water for 90 min under N_2. The produced black liquid containing iron oleate was washed with ethanol and DI water 5 times in a separatory funnel to remove impurities, then dried at 110 ºC in on a hot plate overnight to remove remaining hexane, ethanol, and water. Dried iron oleate is a black, viscous solution that is stored under vacuum.

For MNP synthesis, 3 mmol of iron oleate was placed in a 250-mL three-neck flask and mixed with 6 mL of 1-octadecene, 3 mL of benzyl ether, and oleic acid. To control the size of MNPs, the amount of oleic acid was adjusted.[45] For 24 nm MNPs, 6 mmol of oleic acid was added. The mixture was degassed at 90 ºC under vacuum for 30 min, then heated at 330 ºC under N_2 for 30 min after it reached the reflux point. After cooling, synthesized MNPs were purified by centrifuge in a mixture of ethanol and hexane (ethanol:hexane = 1:4 (v/v)) three times. Washed MNPs were resuspended in 3 mL of chloroform and stored at 4 ºC.

2.2. Magnetic nanodisc synthesis

Magnetic nanodiscs (MNDs) were synthesized according to Gregurec *et al*.[47] Non-magnetic hematite nanodiscs (NDs) were synthesized using the hydrothermal method. 800 mg of sodium acetate and 273 mg of $FeCl_3 \cdot 6H_2O$ were placed in a Teflon vessel. After 10 mL of ethanol and 800 µL of DI water were added, the Teflon vessel was sealed tightly and heated at 180 ºC for 18 hr. The synthesized red solution was washed with ethanol 3 times by centrifuge, and then the pellet of hematite NDs was resuspended in 10 mL of ethanol. The solution was placed under vacuum and dried overnight.

100 mg of the hematite ND power as placed in a 250-mL three-neck flask with 2.22 mL of oleic acid and 29 mL of trioctylamine. The solution was heated at 370 ºC with H_2 bubbling. Heating was stopped 3 min after the color of the solution changed from red to black. The black magnetite NDs (MNDs) were washed with a 1:1 mixture of hexane and ethanol two times and with chloroform three times using magnetic separation. MNDs were resuspended in 1 mL of chloroform and stored at 4º C.

2.3. Silica shell formation on nanomaterials through SCHLR and amine functionalization

2.3.1. Magnetic nanoparticles

The SCHLR method was developed based on the RMM.[24] 25 mL of cyclohexane was placed in a 50-mL falcon tube. In the standard condition, 250 µL of oleic acid and 1540 mg of Igepal CO-520 were added to the tube and shaken to mix. 900 pmol of MNP in chloroform (typically less than 100 µL) was added and mixed well by vortexing. 210 µL of NH_4OH was added to the solution and mixed immediately. To control the thickness of the silica shell, the amount of tetraethyl orthosilicate (TEOS) was adjusted. For a 4 nm-thick silica shell, 4 µL of TEOS was added, followed by vortexing for 48 hr. For amine functionalization, 1 µL of [3-(2-

aminoethylamino)propyl]trimethoxysilane (AEAPTMS) was added to the solution and vortexed another 90 min.

To stop the reaction and purify the silica-coated MNPs, 4 mL of 50 mM tetramethylammonium hydroxide (TMAOH) in methanol was added to the tube. The tube was shaken for 5 sec and allowed to stand for 30 sec, and the black bottom layer was collected in five 1.5 mL Eppendorf tubes and centrifuged at 10,000 kg for 10 min. After the supernatant was removed, the pellet was resuspended in 50 mM TMAOH solution, and the solution was centrifuged at 10,000 g for 10 min. The pellet was resuspended in dimethyl sulfoxide (DMSO) and sonicated, then centrifuged at 20,000 g for 20 min. Repeat this DMSO washing step one more time. The final pellet was resuspended in 400 µL of DMSO and stored at room temperature.

2.3.2. Quantum dots

Quantum dots (QDs) were purchased from Sigma-Aldrich (#919136, 11.5 nm, 5 mg/mL). For silica shell coating of QDs, the same recipe as silica-coated MNPs was applied except for the amount of QDs and TEOS. Typically, 100 µL of QD solution at 5 mg/mL in toluene was added to the reaction solution instead of MNPs. To obtain ~32 nm silica-coated QDs, 6 µL of TEOS was added.

2.3.3. Magnetic nanodiscs

The recipe for MNDs is the same as the one for MNPs except for the amount of MNDs and TEOS. Instead of MNPs, 2.76 mg of MNDs in chloroform was added to the reaction solution. 20 µL of TEOS (3.6 mM) was added to obtain ~4 nm-thick silica shells.

2.4. Functionalization of amine-functionalized silica shells through carbodiimide chemistry

Amine-functionalized silica shells were modified with dyes (Pacific Blue-*N*-Hydroxysuccinimide (PB-NHS): Fluoroprobes #1245-5, Alexa Fluor 488 (AF488)-NHS and Alexa Fluor 568 (AF568)-NHS: Lumiprobe, #11820 and #14820, respectively), methoxy poly(ethylene glycol) (mPEG24-NHS; BroadPharm #BP-23970) or O^6-benzylguanine (BG)-PEG5k-NHS through NHS chemistry. BG-PEG5k-NHS was synthesized via NHS chemistry between BG-NH_2 (AmBeed #A455042) and NHS-PEG5k-NHS (Nanocs, #PG2-THTZ-5k).[48] 1 equivalent amount of NHS-PEG5k-PEG was mixed with 1.5 equivalent amount of BG-NH_2 in DMSO for 18 h. For all types of silica-coated nanomaterials, with a target grafting density of 1 chain/nm^2, a 20-fold excess of ligands was used for NHS chemistry. The particles and ligands were mixed in DMSO on a vortex for 48 hr. The functionalized silica-coated nanomaterials were purified in DI water by 3 rounds of centrifugation at 20,000 g for 20 min and stored at 4 ºC.

2.5. Structural and magnetic characterization

Transmission electron microscope (TEM) images and electron diffraction patterns of all coated/non-coated nanomaterials were obtained with an FEI Tecnai G2 Spirit TWIN TEM. Fiji was used for visualization and size analysis.[49] Dynamic light scattering measurements were performed with a Nicomp Nano DLS/ZLS systems. The concentration of nanomaterials was measured by using an Agilent 5100 Inductively Coupled Plasma-Optical Emission Spectrometer (ICP-OES). Room-temperature hysteresis loops were measured by a vibrating sample magnetometer (VSM, Digital Measurement Systems Model 880A).

Specific loss power (SLP) was measured in a similar method to previously-described (Fig. S6).[50,51] Briefly, 50 µL of sample solutions in DI water (2 mg/mL, n = 3) were placed in small glass vial together with an optical fiber temperature probe (Omega HHTFO-101) and measured.[52]

The air gap between the sample tube and the coil is ~4 cm. Alternating magnetic field was applied with a frequency f = 163 kHz and amplitude H_0 = 35 kA/m. The field amplitude was measured using an inductive pick-up coil installed next to the main coil. As a control measurement, 50 µL of de-ionized (DI) water without MNPs was used, and no temperature change was observed.

2.6. Optical characterization of quantum dots

Optical properties of QDs were measured with a Molecular Devices SpectaMax M2e with using a quartz cuvette. For photoluminescence measurements, excitation wavelength of 475 nm was used. For evaluation of the quantum yield, rhodamine B was used as a standard dye, which has the quantum yield of 0.36 in DI water.[53] The excitation and emission wavelengths for rhodamine B were 565 nm and 590 nm, respectively.

2.7. In vitro genetic cell targeting

12-mm round coverslips (Electron Microscopy Sciences, #72196-12, #1 thickness) were coated with Matrigel (Corning) at a 1:30 dilution by the standard thin coating method provided by the manufacturer and placed in a 24-well plate. HEK293T cells were seeded on the coverslips in 1mL of Dulbecco's Modified Eagle Medium (DMEM, GlutaMAX supplement, Gibco) with 2.5% fetal bovine serum (FBS, Cytiva) and transfected when cells reach 70% confluency by adding a mixture of 4 µL of Lipofectamine 2000 (Invitrogen) and 1 µg of DNA plasmid (*pAAV-CMV::SNAPtm*) in 50 µL of Opti-MEM (Gibco). HEK cells were cultured at 37ºC with 5% CO_2. Media was exchanged for fresh media 6 hr after transfection. 48 hr after transfection, 2 µg of either QD-PEG/BG or QD-PEG in DI water was added to the medium. After incubation with QDs for 15 min, cells were washed with phosphate-buffered saline (PBS) 2 times and then fixed for 15 min in 4% paraformaldehyde in PBS. After three washes with PBS, cells were stained with BioTracker

488 (Sigma-Aldrich) in a 1:1000 dilution in PBS for 15 min. After three washes with PBS, coverslips were mounted onto glass slides using Fluoromount-G (Invitrogen).

Targeting specificity of QD-PEG/BG was evaluated and quantified using a Leica DMI8 Inverted Confocal Microscope. For quantification, a 20x objective lens was used to obtain fluorescence images. For high magnification images, a 60x objective lens was used. QDs were excited with a 400-nm diode laser and detected at 620-660 nm. The images were quantified by using CellProfiler.[54]

2.8. Nanomagnetic simulations

Nanomagnetic Simulations were performed using MuMax3.[55] Particles were 24 nm spheres with edge to edge spacing of 2 nm (from TEM, Fig. 2b). The simulated spheres have a saturation magnetization of 110 emu/$g_{[Fe]}$ (determined via VSM) and were given the exchange constant of magnetite (1.3×10^{-12} J/m).[56] Hysteresis calculations were performed by slightly varying the applied external field and allowing the simulation to relax to its lowest energy state.

3. Results and Discussion

OAc is commonly used as a ligand for nanoparticles to preserve their colloidal stability and prevent aggregation. We hypothesized that the aggregation of OAc-capped nanomaterials during the RMM may partially occur because their surfaces are not fully passivated (due to particle storage or purification steps between their synthesis and coating) (Figure 1a). Introducing OAc into the silica shell coating solution was therefore anticipated to facilitate particle separation and prevent the formation of multi-core assemblies, as it would ensure complete passivation of the

particle surfaces throughout the full RMM procedure. However, because OAc can also act as a surfactant, it was unclear if its inclusion would negatively affect the micelles critical to the RMM approach.[57–59]

To examine the effects of adding OAc ligand to the RMM solution, we first applied a silica coating RMM to spherical Fe_3O_4 magnetic nanoparticles (MNPs) 24 nm in diameter, produced via a common organometallic synthesis that uses OAc for surface passivation (Figure 2a 'MNP 24 nm', S1).[31,46] When these MNPs were directly incorporated into a previously reported RMM, the products comprised <20% single-core particles, and the silica shells exhibited large variations in thickness (Figure 2a '–OAc', 2d). In contrast, when the same protocol and reagents were used, but additional OAc (31.5 mM) was introduced into the coating solution, the emulsion method produced >90% single-core particles with uniform shell thicknesses as corroborated by transmission electron microscopy (TEM) (Figure 2a '+OAc', 2b, S2). The difference in hydrodynamic diameter was also confirmed by dynamic light scattering (DLS) (Figure 2c). These outcomes were consistent across different batches of MNPs and could be independently reproduced by multiple researchers (Figure S3).

Importantly, the prevention of multicore formation was observed over a broad range of OAc additions (6.3 to 75.6 mM OAc). At the lowest concentration, >90% of particles possessed a single MNP per particle, and the fraction of single-cores increased concomitantly with the amount of added OAc. These results are consistent with the hypothesis that additional OAc ensures that all particle surfaces remain saturated with ligand during the silica coating, thereby preventing aggregation (Figure 2d). Moreover, they suggest that this method may simplify the process of adapting the RMM to different particle coatings (*vide supra*), given that the concentration of OAc did not need to be precisely calibrated to prevent multi-core formation. However, we observed an

upper bound to OAc addition that must be considered in using the SCHLR approach, as the addition of 113 mM OAc failed to produce silica-coated particles (Figure S4). We hypothesize that this failure to coat the particles is due to the large amount of hydrophobic ligands in the reaction solution affecting the kinetics of ligand exchange necessary for TEOS to bind to the particle surface and produce a silica coating.[30] This observation is also consistent with the hypothesis that the dynamic nature of OAc binding plays a role in the stability of particles during RMM, and with the observations of prior RMM investigations.[30] For example, Koole et al. observed that CdSe quantum dots embedded in silica were similarly not encapsulated above a critical concentration of an added ligand (dodecanethiol).[30] While this large excess of OAc did impair the silica coating process, our data still indicate that there is a wide range of [OAc] that prevent particle agglomeration during RMM without impairing the silica growth process, indicating that SCHLR is a versatile and straightforward modification to improve silica coating methods.

The effect of OAc on colloidal stability of core particles was further investigated by measuring the nanoparticle hydrodynamic diameter during the silica coating reaction. We observed immediate aggregation upon preparation of the reaction solution (Figure 2e). In the absence of OAc, the hydrodynamic diameter only exhibited modest changes (between 600-800 nm) even after 24 hr. In contrast, in the presence of 17 mM oleic acid, the hydrodynamic diameter decreased to approximately 50 nm after 9 hr, even though initial aggregation behavior was similar to control conditions without excess OAc. Importantly, the timescale of silica condensation (on the order of hours) is significantly slower than the formation of reverse micelles (on the order of milliseconds to seconds).[60–62] Thus, the DLS data indicate that the added OAc improves particle

stability during silica condensation without affecting reverse micelle formation in a manner that would negatively impact MNP phase transfer.

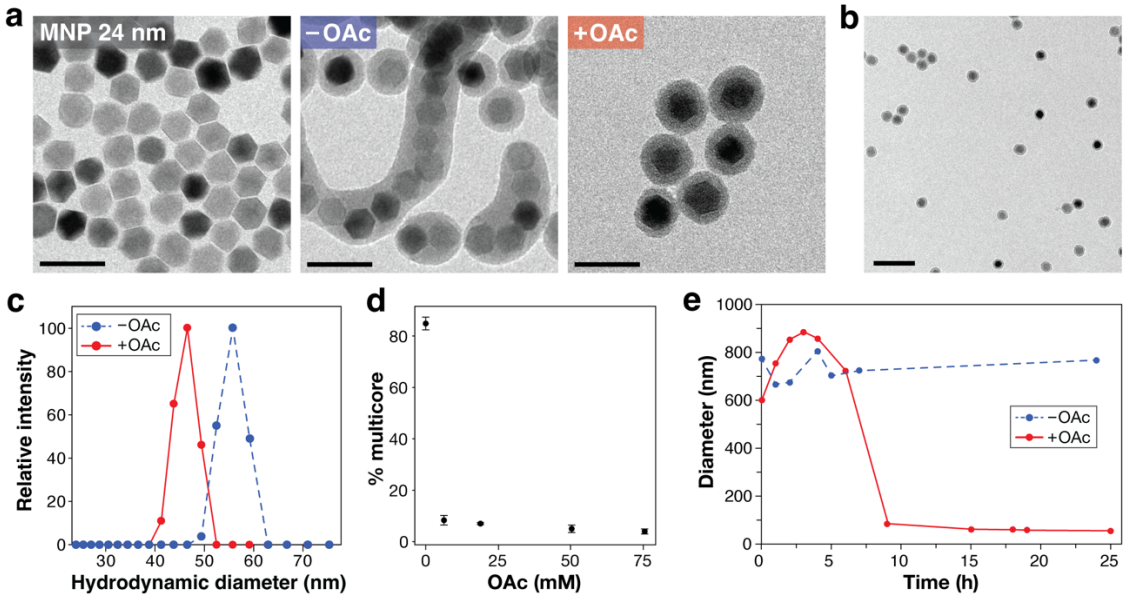

Figure 2. **(a)** TEM images of various silica-coated nanomaterials. The images display bare 24 nm MNPs (left), silica-coated nanomaterials through RMM (middle, labeled '-OAc'), and those produced through the SCHLR method (right, labeled '+OAc'). Scale bars, 50 nm. **(b)** Low magnification TEM image of the same silica-coated MNPs shown in **a "+OAc**'. Scale bar is 100 nm. **(c**) The hydrodynamic diameters of silica-coated 24 nm MNPs measured by dynamic light scattering (DLS). The MNPs were coated using either the conventional method ('-OAc') or the SCHLR method ('+OAc'). **(d)** The relation between the concentration of OAc and proportion of multi-core particles. **(e)** The change in hydrodynamic diameter during the silica shell coating process with ('+OAc') and without oleic acid ('-OAc'), as measured by DLS.

To test the versatility of the SCHLR method, we applied it to nanoparticles of different dimensions, shapes, and compositions. Initially, isotropic Fe_3O_4 MNPs of varying core diameters (20 and 28 nm) were coated using the standard RMM without the addition of OAc to the RMM solution; these MNPs formed multi-core particles and the thickness of the shells were inhomogeneous (Figure 3a, b "-OAc"). In contrast, when these MNPs were coated through the SCHLR method (Figure 3a, b "+OAc", S2), homogeneous shells were formed and minimal

multicore particles were observed. When the SCHLR method was applied to colloidal CdSe/ZhS core-shell quantum dots (QDs, d = 11.5 nm, photoluminescence peak, PL, λ_{PL} = 650 nm), it also produced single-cored, uniformly coated particles (Figure 3c '+OAc'). As with the small ferrite nanoparticles, RMM without OAc produced predominantly multicore aggregates (Figure 3c '-OAc'). Larger Fe_3O_4 magnetic nanodiscs (MNDs, 240.0±23.2 nm in diameter, 28.2±3.9 nm thickness) were also coated with silica through the SCHLR method (Figure 3d 'MND'). Again, the addition of OAc to RMM yielded uniform silica shells on isolated MNDs (Figure 3d '+OAc'). In contrast, in the absence of OAc, the RMM protocol was ineffective, leaving MNDs uncoated and promoting the nucleation of small silica spheres (Figure 3d '-OAc'). We hypothesize that in addition to improving the colloidal stability of MNDs, OAc is affecting the size of the reverse micelles and the fluidity of surfactants that comprise the micellar coating, as a 240 nm MND is too large to be encompassed in a typical Igepal-H_2O reverse micelle, (~45 nm under solution conditions examined here).[63] In the absence of OAc, MNDs do not enter the reverse micelles, which precludes their coating with silica and results in the formation of empty silica spheres seen in the TEM images (Figure 3d '-OAc'). These findings indicate SCHLR is broadly applicable to OAc-capped nanoparticles regardless of size, shape, and composition.

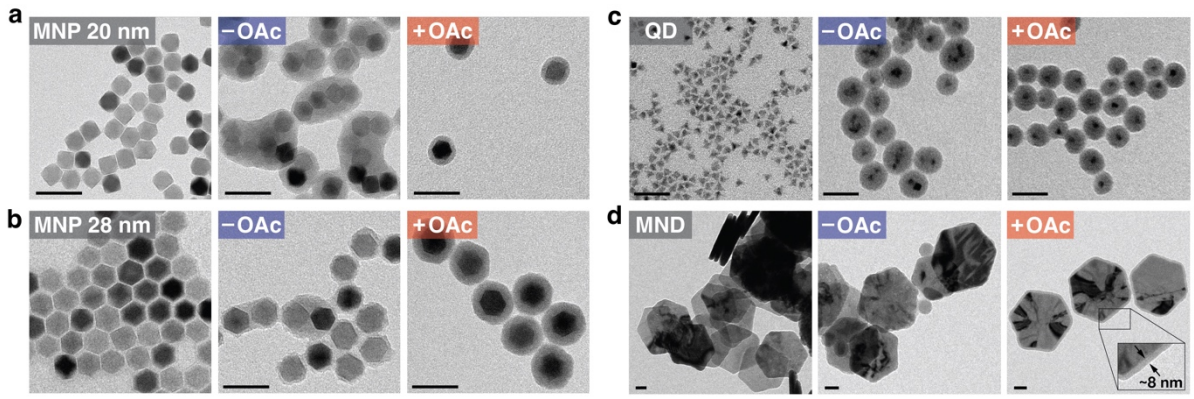

Figure 3. TEM images of various silica-coated 20-nm MNP (**a**), 28-nm MNP (**b**), quantum dots (**c**), and magnetic nanodiscs (**d**). The images display bare nanomaterials (left), silica-coated nanomaterials through RMM (middle, labeled '-OAc'), and those produced through the SCALR method (right, labeled '+OAc'). The synthesis conditions for each panel can be found in Table S2. Scale bars, 50 nm.

In addition to broad nanoparticle composition applicability, the SCHLR method enables precise control over silica-shell thickness. By altering the amount of silica precursor (TEOS), the shell thickness can be linearly tuned between 0.7 nm to 7.7 nm (Figure 4a, b). In contrast, in a standard RMM, precisely controlling silica shell thickness was not possible due to the formation of uneven shells and multi-core particles, especially for larger cores or thinner silica shells.[33,44] Yang et al. hypothesized that the repulsion force between negatively charged hydrophilic nanomaterials is screened by NH_4^+ at a lower concentration of TEOS, leading to the agglomeration of nanomaterials and the formation of multi-core particles.[44] We anticipate that a similar mechanism might be occurring in the SCHLR method. We hypothesize that additional OAc slows the ligand exchange between OAc and TEOS, which allows more hydrolyzed TEOS molecules to accumulate in reverse micelles, thereby weakening the electrostatic screening effect by NH_4^+. As a result, after the first nanoparticle enters a reverse micelle, the inter-particle electrostatic repulsion is strong enough to prevent the entry of other particles into the same micelle.

Silica shell thickness was also observed to correlate to the concentration of OAc. Between OAc concentrations of 5 and 45 mM, the silica shell thickness was inversely correlated with the amount of OAc in solution (Figure 4c, d). No further decrease in shell thickness was observed above OAc concentrations of 45 mM, but silica coating syntheses at higher OAc concentrations also produced silica nanospheres (~5 nm) devoid of nanoparticle cores (Figure 4c). These silica spheres were more numerous at the highest concentrations of OAc. We hypothesize that the addition of extra OAc molecules leads to the formation of small reverse micelles that are composed mainly of OAc molecules that are incapable of incorporating a large nanoparticle. Hydrolyzed TEOS intermediates within these OAc reverse micelles therefore form core-free silica nanospheres. As a result, a portion of the added TEOS is consumed by the formation of silica nanospheres, and the number of TEOS molecules available to coat nanomaterials decreases, resulting in the thinner shells. Silica nanospheres were not observed at smaller OAc concentrations, at which the formation of multi-cores is suppressed (Figure 2d). Notably, unlike prior methods that produced silica spheres of comparable size to the coated nanoparticles, these silica spheres are significantly smaller than the coated nanoparticles and thus can be more readily removed from the sample during subsequent purification steps after functionalization of the silica surface with aminoethylaminopropyltrimethoxysilane as discussed below (Figure 4c “68 mM purified”).

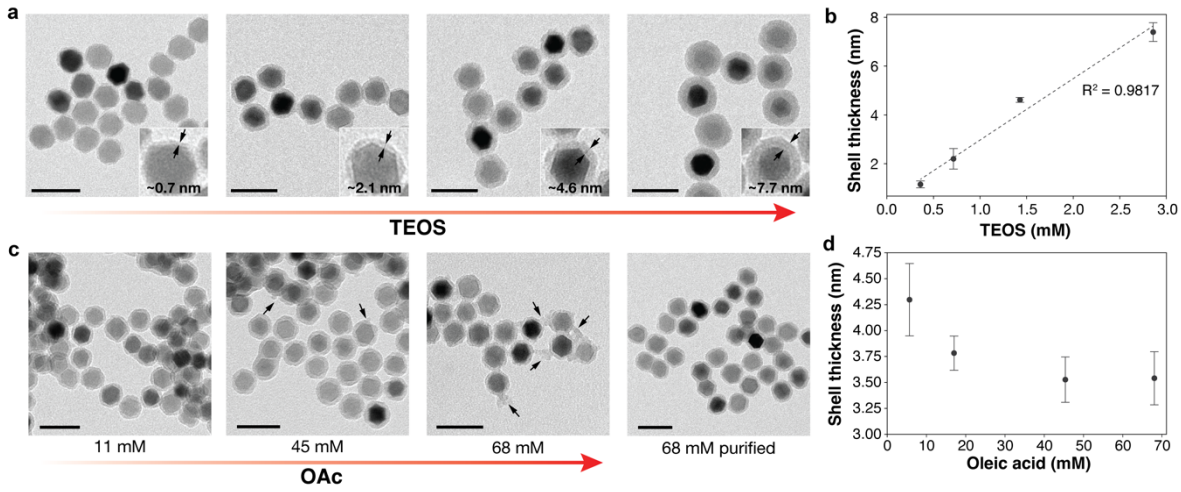

Figure 4. **(a)** TEM images of silica-coated MNPs by SCHLR with different amounts of TEOS. **(b)** The relation between shell thickness and the amount of TEOS (N=3). **(c)** TEM image of silica-coated MNPs at an OAc concentration of 11, 45, and 68 mM. More silica nanospheres (~58 nm) were observed with the amount of OAc added. After purification steps, these silica nanospheres were washed away and no such spheres were observed ("68 mM purified"). **(d)** The relation between shell thickness and concentration of OAc (N=3). The concentration of TEOS was 0.72 mM. Scale bars, 50 nm.

Coating the particles with silica via the SCHLR method does not impair the properties of the nanoparticle cores. For the MNPs, the deposition of silica did not degrade the saturation magnetization (M_s) with the exception of particularly thick (7.6 nm) shells, for which 27% decrease in M_s was observed (Figure 5a, b). This is likely due to partial degradation of MNP cores at large (~3 mM) TEOS concentrations. This is supported by the observation of iron oxide nanodiscs dissolution at TEOS concentrations ~10 times greater (36 mM) than those used for silica-shell deposition (Figure S5). In control samples where MNPs were silica-coated in the absence of OAc, a coercivity increase was observed due to aggregation of particles. The formation of anisotropic multi-core MNP structures imparts uniaxial shape anisotropy that scales with the number of particles (Figure S6).

One of the most common applications of MNPs is in magnetic hyperthermia, and the efficiency of the MNPs' hysteretic heat dissipation in alternating magnetic fields (AMFs) is measured by the specific loss power (SLP in $W/g_{[Fe]}$).[64] SLP was measured at an AMF with a frequency of 165 kHz and amplitudes of 26 and 35 kA/m (Figure 5c). For the low-amplitude AMF condition, SLPs were higher for the MNPs coated with 0.7 nm shells via SCHLR than for the MNPs coated via RMM without the OAc. The SLP of the MNPs coated with thick shells was significantly reduced, which can be attributed to the lower M_s. At the high-amplitude AMF condition, all SLP values increased as expected from the amplitude approaching the coercive field of the particles.[46] Notably, SLPs were higher for the MNPs silica-coated in the absence of OAc. This is consistent with vibrating-sample magnetometer (VSM) measurements that reveal higher coercivity of multi-core particles (–OAc) as compared to single-core particles (+OAc), which manifests in a larger hysteresis loop area. Since the SLP is proportional to the frequency-integrated hysteresis loop area, the difference in heating between –OAc and +OAc is attributed to the ability of the higher (35 kA/m), but not lower (26 kA/m), AMF amplitude to access this entire area.[65]

In addition to magnetic behaviors of MNPs, the spectral characteristics of QDs were measured before and after silica shell coating via SCHLR (Figure 5d, S7). The photoluminescence (PL) spectra were nearly identical with no noticeable degradation or peak shift. The quantum yield (ε) after silica shell coating by SCHLR ($\varepsilon = 0.47$) was comparable to polymer-coated QDs ($\varepsilon = 0.53$). In contrast, a notable degradation in quantum yield was observed when a conventional RMM was used ($\varepsilon = 0.35$).

A uniform surface coating for nanomaterials enables standardization of functionalization protocols to alter their surface chemistry. To demonstrate that the SCHLR method empowers such surface modification, silica shell coated MNPs were functionalized with primary amine groups by

the addition of [3-(2-aminoethylamino)propyl]trimethoxysilane (AEAPTMS) via commonly used protocols.[24] After purification, these amine-functionalized silica-coated MNPs were labeled with fluorescent dyes through carbodiimide chemistry (Figure 5e). Three different dyes, Pacific Blue (PB), Alexa Fluor 488 (AF488), and Alexa Fluor 568 (AF568) with distinct PL excitation and emission profiles ((λ_{ex}, λ_{em}) = (410, 455 nm), (490, 525 nm), and (568, 610 nm)) were linked to MNP surfaces. Each of these dyes maintained their PL characteristics after attachment to the silica-coated MNPs, demonstrating that SCHLR coats nanoparticles in functional surfaces that can be directly incorporated into widely applied functionalization protocols.

To further demonstrate the utility of the SCHLR process in engineering nanomaterial surfaces, we modified silica-coated QDs with moieties that permitted their genetic targeting to cells via SNAP-tag® technology that uses a covalent bonding between O^6-benzylguanine (BG) and a SNAP-tag protein (Figure 5f).[66] This robust and selective approach is commonly employed in biomedical sciences to deliver non-genetic payloads with genetic specificity. Silica-coated QDs were modified with a combination of BG and polyethylene glycol (PEG) via carbodiimide chemistry (QD-PEG/BG). The addition of PEG ensured colloidal stability of BG-functionalized QDs, minimizing non-specific interactions with HEK293 cells, which were chosen as a widely used mammalian cell line. Following incubation with QD-PEG/BG, HEK293 cells expressing SNAP-tag exhibited significant membrane fluorescence, indicative of specific QD binding, while in the absence of SNAP tag or following incubation with QD-PEG lacking BG moiety negligible membrane fluorescence was observed (Figure 5f, g).

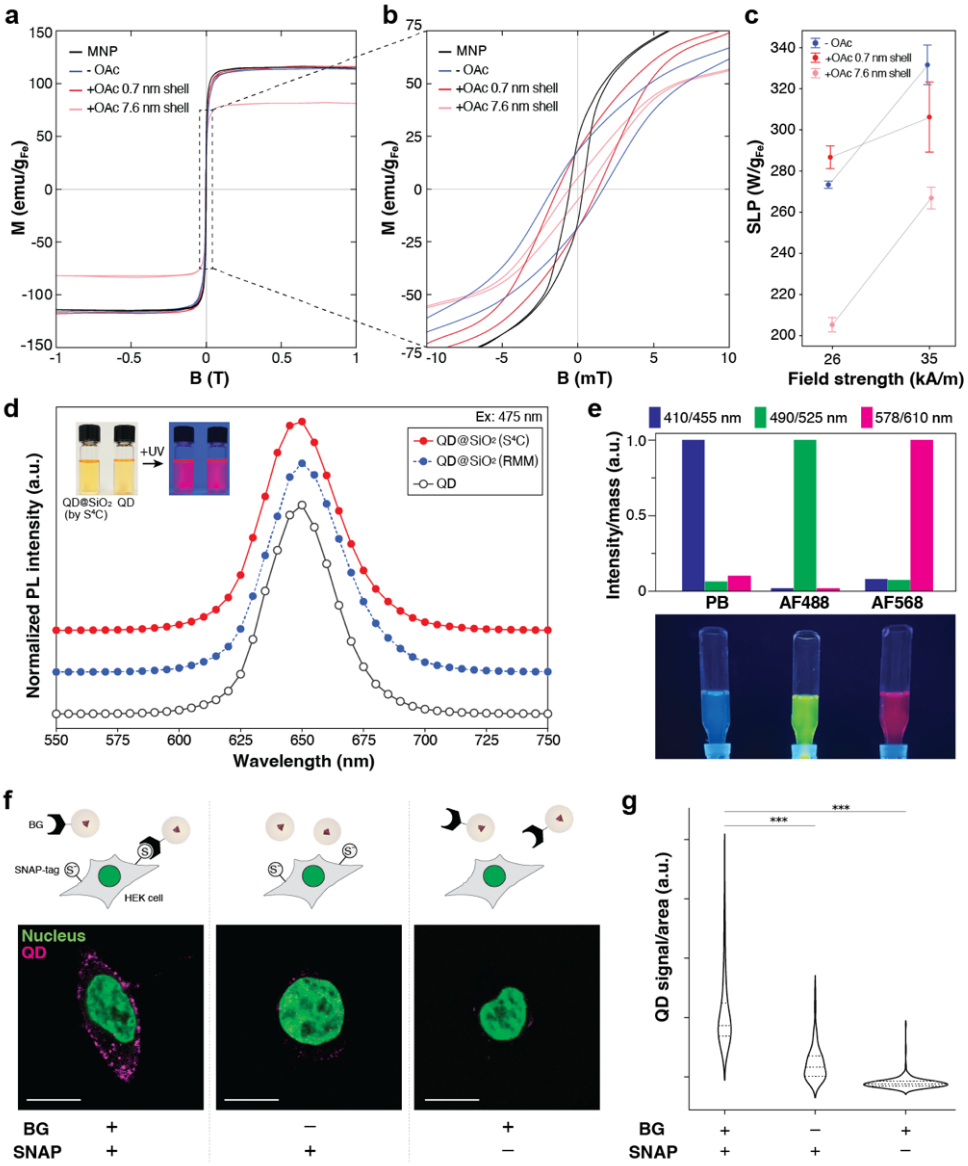

Figure 5. (a, b) Magnetization curves of bare MNPs and silica-coated MNPs. MNP: bare MNPs. -OAc: silica-coated MNPs by the conventional method. +OAc, 0.7 nm shell: silica-coated MNPs by SCHLR with shell thickness 0.7 nm. +OAc, 7.6 nm: silica-coated MNPs by SCHLR with shell thickness 7.6 nm. **(c)** SLP values of silica-coated MNPs. **(d)** Emission spectra of bare QD and silica-coated QD. The excitation wavelength was 475 nm. The concentration of QD is the same across the three conditions. The three plots are offset. **(e)** Fluorescence intensities of dye-labeled silica-coated MNP. The values were normalized by the mass of core MNPs. An image of corresponding dye-labelled MNPs under UV light is provided beneath the bar plot. **(f)** Fluorescence images of HEK cells cultured with BG-functionalized QDs and control cells. The cell nuclei were stained with a green dye (BioTracker green). QDs were excited at 600 nm and imaged in the window of 625 – 655 nm. Scale bars are 10 μm. **(g)** Statistical analysis of the fluorescence intensity from the QDs normalized by cell area. The model used was the Kruskal-Wallis one-way ANOVA. (***P < 0.0001).

4. Conclusion

The RMM is a widely used approach for coating hydrophobic nanomaterials with silica as a means of preventing chemical degradation, simplifying surface ligand engineering, facilitating transfer into aqueous media, and improving biocompatibility. However, the sensitivity of RMM to reaction conditions often manifests in non-uniform shell thickness and aggregation of particles during coating. Here we have demonstrated that the addition of hydrophobic ligand, OAc, to the reaction solution for RMM prevents the formation of multi-core particles, thereby enhancing the uniformity and reproducibility of silica shells. We have also shown that our modified silica coating protocol yields uniform silica shells of tunable thickness, including thin shells (<1 nm) that minimize alterations to overall particle size, shape, and functional properties (Fig. 3-5).

The SCHLR method can be used to silica-coat nanomaterials with different core compositions (e.g. magnetite MNPs and CdSe/ZnS QDs), sizes (11-240 nm), and shapes (e.g. spheres vs. discs). Additionally, the SCHLR silica shells can be readily modified with a variety of moieties through established silica functionalization chemistries, enabling their use in, for example, biomedical applications. The only requisite for SCHLR is the initial nanoparticle passivation with OAc. However, many synthetic protocols for high-quality nanomaterials (MNPs, QDs) are conducted in hydrophobic organic solvents and use OAc as a primary surfactant, indicating potentially broad utility of this approach. We anticipate that silica-coated particles produced via the SCHLR method will empower colloidal nanomaterials research by offering enhanced reproducibility and control over particles' surface properties.

Associated content

Supporting Information

The following files are available free of charge.

Experimental details, supplementary table S1-S3, supplementary figure S1-S8 (PDF)

Author Information

Corresponding Authors

Polina Anikeeva – Department of Materials Science and Engineering, Research Laboratory of Electronics, McGovern Institute for Brain Research, and Department of Brain and Cognitive Sciences, Massachusetts Institute of Technology, Cambridge, Massachusetts 02139, USA; orcid.org/0000-0001-6495-5197; Email: anikeeva@mit.edu

Robert J. Macfarlane – Department of Material Science and Engineering, Massachusetts Institute of Technology, Cambridge, Massachusetts 02139, USA; orcid.org/0000-0001-9449-2680; Email: rmacfarl@mit.edu

Authors

Keisuke Nagao – Department of Materials Science and Engineering, Research Laboratory of Electronics, and McGovern Institute for Brain Research, Massachusetts Institute of Technology, Cambridge, Massachusetts 02139, USA; orcid.org/0009-0002-2296-1817

Katherine Lei – Department of Materials Science and Engineering, Research Laboratory of Electronics, and McGovern Institute for Brain Research, Massachusetts Institute of Technology, Cambridge, Massachusetts 02139, USA

Peyton Worthington – Department of Mechanical Engineering, Research Laboratory of Electronics, and McGovern Institute for Brain Research, Massachusetts Institute of Technology, Cambridge, Massachusetts 02139, USA

Noah Kent – Department of Materials Science and Engineering, Research Laboratory of Electronics, and McGovern Institute for Brain Research, Massachusetts Institute of Technology, Cambridge, Massachusetts 02139, USA

Michika Onoda – Department of Materials Science and Engineering, Massachusetts Institute of Technology, Cambridge, Massachusetts 02139, USA

Elian Malkin – Department of Brain and Cognitive Sciences, Research Laboratory of Electronics, and McGovern Institute for Brain Research, Massachusetts Institute of Technology, Cambridge, Massachusetts 02139, USA

Emmanuel Vargas Paniagua – Research Laboratory of Electronics, and McGovern Institute for Brain Research, Massachusetts Institute of Technology, Cambridge, Massachusetts 02139, USA

Rebecca Leomi – Research Laboratory of Electronics, and McGovern Institute for Brain Research, Massachusetts Institute of Technology, Cambridge, Massachusetts 02139, USA

Present Addresses

†MO – Pure Lithium, Charlestown, Massachusetts 02129, USA

Author Contributions

The manuscript was written through contributions of all authors. All authors have given approval to the final version of the manuscript.

K.N.: Conceptualization, methodology, data collection, formal analysis, visualization, writing. K.L.: Data collection, formal analysis, writing. P.W.: Data collection, formal analysis, writing. N.K.: Magnetic simulation, writing. M.O.: Methodology, writing. E.P.: Data collection, writing. E.M.: Data collection, formal analysis, writing. R.L.: Investigation, writing. R.J.M.: Conceptualization, funding acquisition, investigation, project administration, writing. P.A.: Conceptualization, funding acquisition, investigation, project administration, writing

Notes

The authors have no conflict of interest to disclose.

Acknowledgements

The authors are grateful to T. Hueckel, R. Li, M. Ye, and G. Desroches for their technical advice on the experiments and manuscript preparation. This work was funded in part by the Pioneer Award from the National Institutes of Health and National Institute for Complementary and Integrative Health (DP1-AT011991, P.A.), NIH BRAIN Initiative and the National Institute for Neurological Disorders and Stroke (R01-NS115576, P.A.), McGovern Institute for Brain Research at MIT, and K. Lisa Yang and Hock E. Tan Center for Molecular Therapeutics at MIT (P.A.). R.J.M. acknowledges support from the Army Research Office under award W911NF-23-2-0101. K.N. is a recipient of a scholarship from the Honjo International Scholarship Foundation.

References

(1) Boles, M. A.; Ling, D.; Hyeon, T.; Talapin, D. V. The Surface Science of Nanocrystals. *Nature Mater* **2016**, *15*, 141–153. https://doi.org/10.1038/nmat4526.

(2) Heuer-Jungemann, A.; Feliu, N.; Bakaimi, I.; Hamaly, M.; Alkilany, A.; Chakraborty, I.; Masood, A.; Casula, M. F.; Kostopoulou, A.; Oh, E.; Susumu, K.; Stewart, M. H.; Medintz, I. L.; Stratakis, E.; Parak, W. J.; Kanaras, A. G. The Role of Ligands in the Chemical Synthesis and Applications of Inorganic Nanoparticles. *Chem. Rev.* **2019**, *119* (8), 4819–4880. https://doi.org/10.1021/acs.chemrev.8b00733.

(3) Walkey, C. D.; Olsen, J. B.; Guo, H.; Emili, A.; Chan, W. C. W. Nanoparticle Size and Surface Chemistry Determine Serum Protein Adsorption and Macrophage Uptake. *J. Am. Chem. Soc.* **2012**, *134* (4), 2139–2147. https://doi.org/10.1021/ja2084338.

(4) Bera, D.; Qian, L.; Tseng, T.-K.; Holloway, P. H. Quantum Dots and Their Multimodal Applications: A Review. *Materials* **2010**, *3* (4), 2260–2345. https://doi.org/10.3390/ma3042260.
(5) Dreaden, E. C.; Alkilany, A. M.; Huang, X.; Murphy, C. J.; El-Sayed, M. A. The Golden Age: Gold Nanoparticles for Biomedicine. *Chem. Soc. Rev.* **2012**, *41* (7), 2740–2779. https://doi.org/10.1039/C1CS15237H.
(6) Jun, Y.; Huh, Y.-M.; Choi, J.; Lee, J.-H.; Song, H.-T.; Kim, S.; Yoon, S.; Kim, K.-S.; Shin, J.-S.; Suh, J.-S.; Cheon, J. Nanoscale Size Effect of Magnetic Nanocrystals and Their Utilization for Cancer Diagnosis via Magnetic Resonance Imaging. *J. Am. Chem. Soc.* **2005**, *127* (16), 5732–5733. https://doi.org/10.1021/ja0422155.
(7) Lee, J.-H.; Jang, J.; Choi, J.; Moon, S. H.; Noh, S.; Kim, J.; Kim, J.-G.; Kim, I.-S.; Park, K. I.; Cheon, J. Exchange-Coupled Magnetic Nanoparticles for Efficient Heat Induction. *Nature Nanotech* **2011**, *6* (7), 418–422. https://doi.org/10.1038/nnano.2011.95.
(8) Arvizo, R. R.; Bhattacharyya, S.; Kudgus, R. A.; Giri, K.; Bhattacharya, R.; Mukherjee, P. Intrinsic Therapeutic Applications of Noble Metal Nanoparticles: Past, Present and Future. *Chem. Soc. Rev.* **2012**, *41* (7), 2943. https://doi.org/10.1039/c2cs15355f.
(9) Chinnathambi, S.; Shirahata, N. Recent Advances on Fluorescent Biomarkers of Near-Infrared Quantum Dots for *in Vitro* and *in Vivo* Imaging. *Science and Technology of Advanced Materials* **2019**, *20* (1), 337–355. https://doi.org/10.1080/14686996.2019.1590731.
(10) Chen, R.; Romero, G.; Christiansen, M. G.; Mohr, A.; Anikeeva, P. Wireless Magnetothermal Deep Brain Stimulation. *Science* **2015**, *347* (6229), 1477–1480. https://doi.org/10.1126/science.1261821.
(11) Lee, J.; Shin, W.; Lim, Y.; Kim, J.; Kim, W. R.; Kim, H.; Lee, J.-H.; Cheon, J. Non-Contact Long-Range Magnetic Stimulation of Mechanosensitive Ion Channels in Freely Moving Animals. *Nat. Mater.* **2021**, *20* (7), 1029–1036. https://doi.org/10.1038/s41563-020-00896-y.
(12) Chen, S.; Weitemier, A. Z.; Zeng, X.; He, L.; Wang, X.; Tao, Y.; Huang, A. J. Y.; Hashimotodani, Y.; Kano, M.; Iwasaki, H.; Parajuli, L. K.; Okabe, S.; Teh, D. B. L.; All, A. H.; Tsutsui-Kimura, I.; Tanaka, K. F.; Liu, X.; McHugh, T. J. Near-Infrared Deep Brain Stimulation via Upconversion Nanoparticle–Mediated Optogenetics. **2018**.
(13) Huang, Y.-W.; Cambre, M.; Lee, H.-J. The Toxicity of Nanoparticles Depends on Multiple Molecular and Physicochemical Mechanisms. *IJMS* **2017**, *18* (12), 2702. https://doi.org/10.3390/ijms18122702.
(14) Marques, A. C.; Costa, P. J.; Velho, S.; Amaral, M. H. Functionalizing Nanoparticles with Cancer-Targeting Antibodies: A Comparison of Strategies. *Journal of Controlled Release* **2020**, *320*, 180–200. https://doi.org/10.1016/j.jconrel.2020.01.035.
(15) Mitchell, M. J.; Billingsley, M. M.; Haley, R. M.; Wechsler, M. E.; Peppas, N. A.; Langer, R. Engineering Precision Nanoparticles for Drug Delivery. *Nat Rev Drug Discov* **2021**, *20* (2), 101–124. https://doi.org/10.1038/s41573-020-0090-8.
(16) Smith, A. M.; Duan, H.; Rhyner, M. N.; Ruan, G.; Nie, S. A Systematic Examination of Surface Coatings on the Optical and Chemical Properties of Semiconductor Quantum Dots. *Phys. Chem. Chem. Phys.* **2006**, *8* (33), 3895. https://doi.org/10.1039/b606572b.
(17) Yan, D.; Shi, T.; Zang, Z.; Zhou, T.; Liu, Z.; Zhang, Z.; Du, J.; Leng, Y.; Tang, X. Ultrastable $CsPbBr_3$ Perovskite Quantum Dot and Their Enhanced Amplified Spontaneous Emission by

Surface Ligand Modification. *Small* **2019**, *15* (23), 1901173. https://doi.org/10.1002/smll.201901173.
(18) Kang, H.; Buchman, J. T.; Rodriguez, R. S.; Ring, H. L.; He, J.; Bantz, K. C.; Haynes, C. L. Stabilization of Silver and Gold Nanoparticles: Preservation and Improvement of Plasmonic Functionalities. *Chem. Rev.* **2019**, *119* (1), 664–699. https://doi.org/10.1021/acs.chemrev.8b00341.
(19) Zeng, J.; Jing, L.; Hou, Y.; Jiao, M.; Qiao, R.; Jia, Q.; Liu, C.; Fang, F.; Lei, H.; Gao, M. Anchoring Group Effects of Surface Ligands on Magnetic Properties of Fe_3O_4 Nanoparticles: Towards High Performance MRI Contrast Agents. *Advanced Materials* **2014**, *26* (17), 2694–2698. https://doi.org/10.1002/adma.201304744.
(20) Vestal, C. R.; Zhang, Z. J. Effects of Surface Coordination Chemistry on the Magnetic Properties of $MnFe_2O_4$ Spinel Ferrite Nanoparticles. *J. Am. Chem. Soc.* **2003**, *125* (32), 9828–9833. https://doi.org/10.1021/ja035474n.
(21) Abdul Jalil, R.; Zhang, Y. Biocompatibility of Silica Coated $NaYF_4$ Upconversion Fluorescent Nanocrystals. *Biomaterials* **2008**, *29* (30), 4122–4128. https://doi.org/10.1016/j.biomaterials.2008.07.012.
(22) Malvindi, M. A.; De Matteis, V.; Galeone, A.; Brunetti, V.; Anyfantis, G. C.; Athanassiou, A.; Cingolani, R.; Pompa, P. P. Toxicity Assessment of Silica Coated Iron Oxide Nanoparticles and Biocompatibility Improvement by Surface Engineering. *PLoS ONE* **2014**, *9* (1), e85835. https://doi.org/10.1371/journal.pone.0085835.
(23) Heitsch, A. T.; Smith, D. K.; Patel, R. N.; Ress, D.; Korgel, B. A. Multifunctional Particles: Magnetic Nanocrystals and Gold Nanorods Coated with Fluorescent Dye-Doped Silica Shells. *Journal of Solid State Chemistry* **2008**, *181* (7), 1590–1599. https://doi.org/10.1016/j.jssc.2008.05.002.
(24) Kim, J.; Seo, D.; Lee, J.; Southard, K. M.; Lim, Y.; Kim, D.; Gartner, Z. J.; Jun, Y.; Cheon, J. Single-Cell Mechanogenetics Using Monovalent Magnetoplasmonic Nanoparticles. *Nat Protoc* **2017**, *12* (9), 1871–1889. https://doi.org/10.1038/nprot.2017.071.
(25) Goftman, V. V.; Aubert, T.; Ginste, D. V.; Van Deun, R.; Beloglazova, N. V.; Hens, Z.; De Saeger, S.; Goryacheva, I. Yu. Synthesis, Modification, Bioconjugation of Silica Coated Fluorescent Quantum Dots and Their Application for Mycotoxin Detection. *Biosensors and Bioelectronics* **2016**, *79*, 476–481. https://doi.org/10.1016/j.bios.2015.12.079.
(26) Darbandi, M.; Thomann, R.; Nann, T. Single Quantum Dots in Silica Spheres by Microemulsion Synthesis. *Chem. Mater.* **2005**, *17* (23), 5720–5725. https://doi.org/10.1021/cm051467h.
(27) Ding, H. L.; Zhang, Y. X.; Wang, S.; Xu, J. M.; Xu, S. C.; Li, G. H. Fe_3O_4 @SiO_2 Core/Shell Nanoparticles: The Silica Coating Regulations with a Single Core for Different Core Sizes and Shell Thicknesses. *Chem. Mater.* **2012**, *24* (23), 4572–4580. https://doi.org/10.1021/cm302828d.
(28) Vogt, C.; Toprak, M. S.; Muhammed, M.; Laurent, S.; Bridot, J.-L.; Müller, R. N. High Quality and Tuneable Silica Shell–Magnetic Core Nanoparticles. *J Nanopart Res* **2010**, *12* (4), 1137–1147. https://doi.org/10.1007/s11051-009-9661-7.
(29) Jang, E.-S. Preparation of Fe_3O_4/SiO_2 Core/Shell Nanoparticles with Ultrathin Silica Layer. *Journal of the Korean Chemical Society* **2012**, *56* (4), 478–483. https://doi.org/10.5012/JKCS.2012.56.4.478.
(30) Koole, R.; van Schooneveld, M. M.; Hilhorst, J.; de Mello Donegá, C.; Hart, D. C. 't; van Blaaderen, A.; Vanmaekelbergh, D.; Meijerink, A. On the Incorporation Mechanism of

Hydrophobic Quantum Dots in Silica Spheres by a Reverse Microemulsion Method. *Chem. Mater.* **2008**, *20* (7), 2503–2512. https://doi.org/10.1021/cm703348y.
(31) Chen, R.; Christiansen, M. G.; Anikeeva, P. Maximizing Hysteretic Losses in Magnetic Ferrite Nanoparticles *via* Model-Driven Synthesis and Materials Optimization. *ACS Nano* **2013**, *7* (10), 8990–9000. https://doi.org/10.1021/nn4035266.
(32) Park, J.; An, K.; Hwang, Y.; Park, J.-G.; Noh, H.-J.; Kim, J.-Y.; Park, J.-H.; Hwang, N.-M.; Hyeon, T. Ultra-Large-Scale Syntheses of Monodisperse Nanocrystals. *Nature Mater* **2004**, *3* (12), 891–895. https://doi.org/10.1038/nmat1251.
(33) Lee, D. C.; Mikulec, F. V.; Pelaez, J. M.; Koo, B.; Korgel, B. A. Synthesis and Magnetic Properties of Silica-Coated FePt Nanocrystals. *J. Phys. Chem. B* **2006**, *110* (23), 11160–11166. https://doi.org/10.1021/jp060974z.
(34) Wang, J.; Tsuzuki, T.; Sun, L.; Wang, X. Reverse Microemulsion-Mediated Synthesis of SiO_2-Coated ZnO Composite Nanoparticles: Multiple Cores with Tunable Shell Thickness. *ACS Appl. Mater. Interfaces* **2010**, *2* (4), 957–960. https://doi.org/10.1021/am100051z.
(35) Selvan, S. T.; Tan, T. T.; Ying, J. Y. Robust, Non-Cytotoxic, Silica-Coated CdSe Quantum Dots with Efficient Photoluminescence. *Adv. Mater.* **2005**, *17* (13), 1620–1625. https://doi.org/10.1002/adma.200401960.
(36) Wang, H.; Schaefer, K.; Moeller, M. In Situ Immobilization of Gold Nanoparticle Dimers in Silica Nanoshell by Microemulsion Coalescence. *J. Phys. Chem. C* **2008**, *112* (9), 3175–3178. https://doi.org/10.1021/jp7113658.
(37) Ureña-Horno, E.; Kyriazi, M.-E.; Kanaras, A. G. A Method for the Growth of Uniform Silica Shells on Different Size and Morphology Upconversion Nanoparticles. *Nanoscale Adv.* **2021**, *3* (12), 3522–3529. https://doi.org/10.1039/D0NA00858C.
(38) Fernández-López, C.; Mateo-Mateo, C.; Álvarez-Puebla, R. A.; Pérez-Juste, J.; Pastoriza-Santos, I.; Liz-Marzán, L. M. Highly Controlled Silica Coating of PEG-Capped Metal Nanoparticles and Preparation of SERS-Encoded Particles. *Langmuir* **2009**, *25* (24), 13894–13899. https://doi.org/10.1021/la9016454.
(39) *Nanomaterial Interfaces in Biology: Methods and Protocols*; Bergese, P., Hamad-Schifferli, K., Eds.; Methods in Molecular Biology; Humana Press: Totowa, NJ, 2013; Vol. 1025. https://doi.org/10.1007/978-1-62703-462-3.
(40) Liz-Marzán, L. M.; Giersig, M.; Mulvaney, P. Synthesis of Nanosized Gold−Silica Core−Shell Particles. *Langmuir* **1996**, *12* (18), 4329–4335. https://doi.org/10.1021/la9601871.
(41) Vanderkooy, A.; Chen, Y.; Gonzaga, F.; Brook, M. A. Silica Shell/Gold Core Nanoparticles: Correlating Shell Thickness with the Plasmonic Red Shift upon Aggregation. *ACS Appl. Mater. Interfaces* **2011**, *3* (10), 3942–3947. https://doi.org/10.1021/am200825f.
(42) Zhu, Y.; Jiang, F. Y.; Chen, K.; Kang, F.; Tang, Z. K. Modified Reverse Microemulsion Synthesis for Iron Oxide/Silica Core–Shell Colloidal Particles. *J Sol-Gel Sci Technol* **2013**, *66* (1), 180–186. https://doi.org/10.1007/s10971-013-2985-x.
(43) Graf, C.; Vossen, D. L. J.; Imhof, A.; Van Blaaderen, A. A General Method To Coat Colloidal Particles with Silica. *Langmuir* **2003**, *19* (17), 6693–6700. https://doi.org/10.1021/la0347859.
(44) Yang, Y.; Jing, L.; Yu, X.; Yan, D.; Gao, M. Coating Aqueous Quantum Dots with Silica via Reverse Microemulsion Method: Toward Size-Controllable and Robust Fluorescent Nanoparticles. *Chem. Mater.* **2007**, *19* (17), 4123–4128. https://doi.org/10.1021/cm070798m.

(45) Chen, R.; Christiansen, M. G.; Sourakov, A.; Mohr, A.; Matsumoto, Y.; Okada, S.; Jasanoff, A.; Anikeeva, P. High-Performance Ferrite Nanoparticles through Nonaqueous Redox Phase Tuning. *Nano Lett.* **2016**, *16* (2), 1345–1351. https://doi.org/10.1021/acs.nanolett.5b04761.
(46) Moon, J.; Christiansen, M. G.; Rao, S.; Marcus, C.; Bono, D. C.; Rosenfeld, D.; Gregurec, D.; Varnavides, G.; Chiang, P.; Park, S.; Anikeeva, P. Magnetothermal Multiplexing for Selective Remote Control of Cell Signaling. *Adv. Funct. Mater.* **2020**, *30* (36), 2000577. https://doi.org/10.1002/adfm.202000577.
(47) Gregurec, D.; Senko, A. W.; Chuvilin, A.; Reddy, P. D.; Sankararaman, A.; Rosenfeld, D.; Chiang, P.-H.; Garcia, F.; Tafel, I.; Varnavides, G.; Ciocan, E.; Anikeeva, P. Magnetic Vortex Nanodiscs Enable Remote Magnetomechanical Neural Stimulation. *ACS Nano* **2020**, *14* (7), 8036–8045. https://doi.org/10.1021/acsnano.0c00562.
(48) Wichner, S. M.; Mann, V. R.; Powers, A. S.; Segal, M. A.; Mir, M.; Bandaria, J. N.; DeWitt, M. A.; Darzacq, X.; Yildiz, A.; Cohen, B. E. Covalent Protein Labeling and Improved Single-Molecule Optical Properties of Aqueous CdSe/CdS Quantum Dots. *ACS Nano* **2017**, *11* (7), 6773–6781. https://doi.org/10.1021/acsnano.7b01470.
(49) Schindelin, J.; Arganda-Carreras, I.; Frise, E.; Kaynig, V.; Longair, M.; Pietzsch, T.; Preibisch, S.; Rueden, C.; Saalfeld, S.; Schmid, B.; Tinevez, J.-Y.; White, D. J.; Hartenstein, V.; Eliceiri, K.; Tomancak, P.; Cardona, A. Fiji: An Open-Source Platform for Biological-Image Analysis. *Nat Methods* **2012**, *9* (7), 676–682. https://doi.org/10.1038/nmeth.2019.
(50) Rosenfeld, D.; Senko, A. W.; Moon, J.; Yick, I.; Varnavides, G.; Gregureć, D.; Koehler, F.; Chiang, P.-H.; Christiansen, M. G.; Maeng, L. Y.; Widge, A. S.; Anikeeva, P. Transgene-Free Remote Magnetothermal Regulation of Adrenal Hormones. *Sci. Adv.* **2020**, *6* (15), eaaz3734. https://doi.org/10.1126/sciadv.aaz3734.
(51) Christiansen, M. G.; Howe, C. M.; Bono, D. C.; Perreault, D. J.; Anikeeva, P. Practical Methods for Generating Alternating Magnetic Fields for Biomedical Research. *Review of Scientific Instruments* **2017**, *88* (8), 084301. https://doi.org/10.1063/1.4999358.
(52) Rosenfeld, D.; Field, H.; Kim, Y. J.; Pang, K. K. L.; Nagao, K.; Koehler, F.; Anikeeva, P. Magnetothermal Modulation of Calcium-Dependent Nerve Growth. *Adv Funct Materials* **2022**, *32* (50), 0224558. https://doi.org/10.1002/adfm.202204558.
(53) Zhang, X.-F.; Zhang, Y.; Liu, L. Fluorescence Lifetimes and Quantum Yields of Ten Rhodamine Derivatives: Structural Effect on Emission Mechanism in Different Solvents. *Journal of Luminescence* **2014**, *145*, 448–453. https://doi.org/10.1016/j.jlumin.2013.07.066.
(54) Stirling, D. R.; Swain-Bowden, M. J.; Lucas, A. M.; Carpenter, A. E.; Cimini, B. A.; Goodman, A. CellProfiler 4: Improvements in Speed, Utility and Usability. *BMC Bioinformatics* **2021**, *22* (1), 433. https://doi.org/10.1186/s12859-021-04344-9.
(55) Vansteenkiste, A.; Leliaert, J.; Dvornik, M.; Helsen, M.; Garcia-Sanchez, F.; Van Waeyenberge, B. The Design and Verification of MuMax3. *AIP Advances* **2014**, *4* (10), 107133. https://doi.org/10.1063/1.4899186.
(56) Lavorato, G.; Winkler, E.; Rivas-Murias, B.; Rivadulla, F. Thickness Dependence of Exchange Coupling in Epitaxial Fe_3O_4 / $CoFe_2O_4$ Soft/Hard Magnetic Bilayers. *Phys. Rev. B* **2016**, *94* (5), 054405. https://doi.org/10.1103/PhysRevB.94.054405.
(57) Kittipongpittaya, K.; Panya, A.; McClements, D. J.; Decker, E. A. Impact of Free Fatty Acids and Phospholipids on Reverse Micelles Formation and Lipid Oxidation in Bulk Oil. *J Americ Oil Chem Soc* **2014**, *91* (3), 453–462. https://doi.org/10.1007/s11746-013-2388-8.
(58) Chaiyasit, W.; Stanley, C. B.; Strey, H. H.; McClements, D. J.; Decker, E. A. Impact of Surface Active Compounds on Iron Catalyzed Oxidation of Methyl Linolenate in AOT–

Water–Hexadecane Systems. *Food Biophysics* **2007**, *2* (2–3), 57–66. https://doi.org/10.1007/s11483-007-9031-x.
(59) Sugiura, S.; Ichikawa, S.; Sano, Y.; Nakajima, M.; Liu, X. Q.; Seki, M.; Furusaki, S. Formation and Characterization of Reversed Micelles Composed of Phospholipids and Fatty Acids. *Journal of Colloid and Interface Science* **2001**, *240* (2), 566–572. https://doi.org/10.1006/jcis.2001.7703.
(60) Chang, C.-L.; Fogler, H. S. Kinetics of Silica Particle Formation in Nonionic W/ 0 Microemulsions from TEOS. *AIChE Journal* **1996**, *42* (11).
(61) Penttilä, P. A.; Vierros, S.; Utriainen, K.; Carl, N.; Rautkari, L.; Sammalkorpi, M.; Österberg, M. Phospholipid-Based Reverse Micelle Structures in Vegetable Oil Modified by Water Content, Free Fatty Acid, and Temperature. *Langmuir* **2019**, acs.langmuir.9b01135. https://doi.org/10.1021/acs.langmuir.9b01135.
(62) Arsene, M.-L.; Răut, I.; Călin, M.; Jecu, M.-L.; Doni, M.; Gurban, A.-M. Versatility of Reverse Micelles: From Biomimetic Models to Nano (Bio)Sensor Design. *Processes* **2021**, *9* (2), 345. https://doi.org/10.3390/pr9020345.
(63) Arriagada, F. J.; Osseo-Asare, K. Controlled Hydrolysis of Tetraethoxysilane in a Nonionic Water-in-Oil Microemulsion: A Statistical Model of Silica Nucleation. *Colloids and Surfaces A: Physicochemical and Engineering Aspects* **1999**, *154* (3), 311–326. https://doi.org/10.1016/S0927-7757(98)00870-X.
(64) Hergt, R.; Dutz, S.; Müller, R.; Zeisberger, M. Magnetic Particle Hyperthermia: Nanoparticle Magnetism and Materials Development for Cancer Therapy. *J. Phys.: Condens. Matter* **2006**, *18* (38), S2919–S2934. https://doi.org/10.1088/0953-8984/18/38/S26.
(65) Carrey, J.; Mehdaoui, B.; Respaud, M. Simple Models for Dynamic Hysteresis Loop Calculations of Magnetic Single-Domain Nanoparticles: Application to Magnetic Hyperthermia Optimization. *Journal of Applied Physics* **2011**, *109* (8), 083921. https://doi.org/10.1063/1.3551582.
(66) Keppler, A.; Gendreizig, S.; Gronemeyer, T.; Pick, H.; Vogel, H.; Johnsson, K. A General Method for the Covalent Labeling of Fusion Proteins with Small Molecules in Vivo. *Nat Biotechnol* **2003**, *21* (1), 86–89. https://doi.org/10.1038/nbt765.

Table of Contents (ToC) Graphic